Available online at www.sciencedirect.com
ScienceDirect
Journal of the European Ceramic Society 28 (2008) 437–445
www.elsevier.com/locate/jeurceramsoc

Functionally graded chemical vapor deposited mullite environmental barrier coatings for Si-based ceramics

S.N. Basu *, T. Kulkarni, H.Z. Wang, V.K. Sarin

Department of Manufacturing Engineering, Boston University, Brookline, MA 02446, USA

Available online 6 April 2007

Abstract

Dense, uniform, crystalline mullite ($3Al_2O_3{\cdot}2SiO_2$) environmental barrier coatings have been deposited by chemical vapor deposition on SiC substrates, using the $AlCl_3$–$SiCl_4$–CO_2–H_2 system. These coatings have exhibited excellent high temperature oxidation and hot-corrosion resistance. For very long-term exposures, it is desirable to reduce the silica activity at the coating surface. A graded coating composition has been achieved in the coatings, with the Al/Si ratio being stoichiometric (∼3) at the coating/substrate interface for coefficient of thermal expansion (CTE) match, and increasing monotonically towards the outer coating surface to some of highest alumina-rich mullite reported to date. The structure of the high alumina mullite has been examined by high-resolution transmission electron microscopy. The effects of the CVD deposition parameters on the coating microstructure and growth kinetics have been investigated.

Keywords: Electron microscopy; Corrosion; Mullite; Functionally graded

1. Introduction

It is projected that the increase in demand for electricity in the United States will be around 80 GW in the next decade.[1] A significant portion of this increased demand will be met by advanced gas turbine systems running at higher temperatures for more efficient and environmentally friendly operation. The current generation of superalloys with thermal barrier coatings has been driven close to their high temperature limit. It is expected that Si-based ceramics, SiC and Si_3N_4, will be introduced in the hot-sections of gas turbines in the next generation of higher operating temperature gas turbines. Already, Si-based ceramics are being widely used in microturbines that provide onsite power generation.

SiC and Si_3N_4 form a protective SiO_2 layer at the surface during high temperature exposure. However, when used in environments found in gas turbine applications, these materials have two major limitations. The presence of elements such as Na, Va and S in combustion environments leads to the formation of corrosive oxides such as Na_2O, V_2O_5, SO_2 and SO_3 which react with the existing protective silica scales to form low melting temperature silicates, leading to severe pit formation, material loss and increased porosity.[2] Furthermore, the high-pressure steam, present in the high-velocity combustion gases, volatilizes the protective silica scale to gaseous Si–O–H species.[3] The loss of the protective oxide leads to an accelerated oxidation of the ceramic surface to SiO_2, which in turn volatilizes again. This repeated cycling of oxidation and volatilization leads to a rapid recession of the surface of the Si-based ceramic.

In order to eliminate hot corrosion and recession, environmental barrier coatings (EBCs) are needed. Mullite ($3Al_2O_3{\cdot}2SiO_2$) has received considerable attention as a potential coating material for silicon-based ceramics due to its excellent corrosion resistance, creep resistance, high temperature strength, and most critically, excellent CTE match, especially with SiC.[4–6] Several processing techniques have been explored to deposit mullite coatings, which need to be microstructurally homogeneous, crystalline, and crack and pore free. Plasma sprayed[5] mullite coatings have been deposited on monolithic SiC and SiC/SiC composite substrates for hot-corrosion protection. It was found that conventional plasma spraying led to a large amount of amorphous phase in the coating. On heating at 1100 °C, these phases crystallized, leading to excessive cracking and debonding due to the accompanying volumetric contraction. This problem was partially ameliorated by heating the substrate, which eliminated the formation

* Corresponding author. Tel.: +1 617 353 6728; fax: +1 617 353 5548.
E-mail address: basu@bu.edu (S.N. Basu).

0955-2219/$ – see front matter © 2007 Elsevier Ltd. All rights reserved.
doi:10.1016/j.jeurceramsoc.2007.03.007

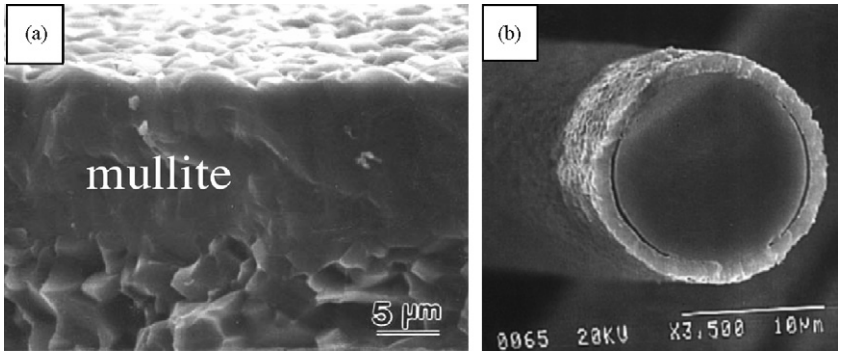

Fig. 1. (a) SEM micrograph of a fracture cross-section of a dense adherent and uniform mullite coating on SiC. (b) Fracture cross-section of a uniform 2 μm thick CVD mullite coating on a 15 μm diameter Nicalon SiC. The partial separation at the fiber/coating interface is due to mechanical stresses in creating the fracture cross-section.

of amorphous phases.[5] Current state-of-the-art environmental barrier coatings are deposited by plasma spraying and have multiphase–multilayered structures that include mullite and a low silica activity barium–strontium–aluminum silicate (BSAS) phase to reduce the preferential volatilization of the silica phase.[6]

2. CVD mullite coatings

2.1. Coating deposition

Mullite coatings were deposited on SiC substrates using the $AlCl_3$–$SiCl_3$–CO_2–H_2 system in a hot-wall CVD reactor.[7] The overall reaction for the deposition process can be described as:

$$6AlCl_3(g) + 2SiCl_3(g) + 13CO_2(g) + 13H_2(g) \rightarrow 3Al_2O_3{\cdot}2SiO_2(s) + 13CO(g) + 26HCl(g) \quad (1)$$

Detailed thermodynamic analysis of the $AlCl_3$–$SiCl_4$–CO_2–H_2 system was carried out to identify the parameters to be used for CVD mullite growth.[8] Based on the thermodynamic calculations, CVD ternary phase diagrams were constructed for the $AlCl_3$, $SiCl_4$ and CO_2 system for various partial pressures of H_2. The analysis showed that CVD mullite deposition should be carried out in the CO_2 rich regime to avoid the incorporation of C and carbides in the coating. In addition, the deposition efficiency (fraction of Al and Si in the input chlorides ending up as mullite) of mullite was also calculated for the different input conditions. It was found that deposition below 800 °C favors the formation of sillimanite over mullite, and that deposition above 1200 °C did not improve the deposition efficiency of mullite. Since chemical equilibrium is rarely achieved in CVD processing, these results were mainly used to establish guidelines in the form of trends, which helped identify the range of process parameters to be explored experimentally.

The SiC samples were hung vertically in the hot zone of the CVD reactor. $AlCl_3$ vapor was produced by passing Cl_2 gas over heated Al chips, while $SiCl_4$ vapor was produced by heating liquid $SiCl_4$ and using Ar as a carrier gas. The metal chlorides ($AlCl_3$ and $SiCl_4$) were pre-mixed before being introduced into the hot zone of the CVD reactor for mullite deposition on SiC substrates described by Eq. (1). The gaseous products were then passed through a neutralizing tank and a chill shower before release into the atmosphere. The typical deposition temperature, total reactor pressure and deposition time were 975 °C, 75 Torr and 3 h, respectively.

2.2. Coating microstructure

Fig. 1 shows a fracture cross-section of a typical uniform mullite coating on a SiC substrate. The figure shows that the coating is dense, uniform and adherent. X-ray diffraction analysis of the coating (Fig. 2) showed the coating to be phase-pure mullite. The CVD process has the ability to deposit uniform coatings on parts with complex shapes. Thus, this process is ideally suited to coat thin fibers, whose surfaces have large curvatures. Fine (∼15 μm diameter) SiC fibers were uniformly coated with mullite using the CVD technique.[9] Fig. 1b shows a SEM micrograph of the coating cross-section on a fractured fiber. These coatings showed excellent adhesion and did not spall even when the fibers were fractured in shear. It is thus evident that the CVD technique can deposit uniform, pore-free, crystalline and phase-pure mullite coatings on SiC substrates with complex geometries.

2.3. Oxidation resistance

The mullite coatings on SiC fibers were very effective in providing high temperature oxidation resistance. Fig. 3 shows a plot of weight gain as a function of oxidation time for SiC

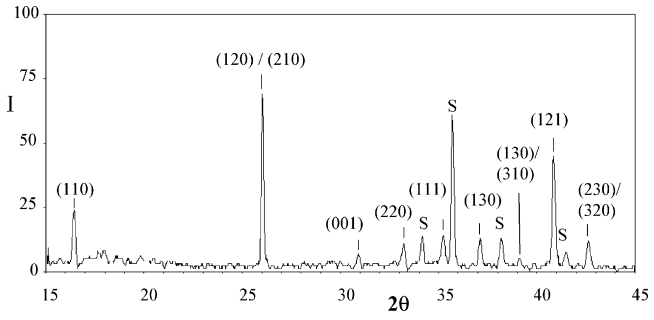

Fig. 2. A θ–2θ X-ray diffraction scan showing that the coating is phase-pure mullite. The substrate peaks are marked as S.

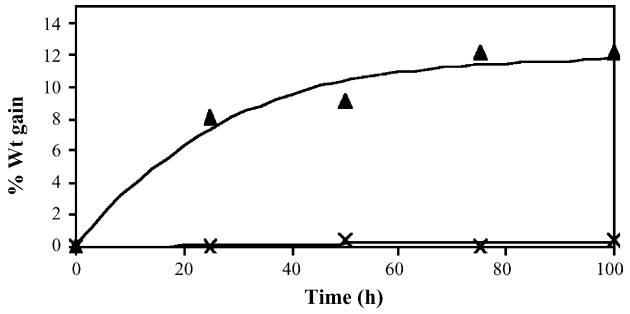

Fig. 3. Weight gain vs. time plots for uncoated (filled Δ) and mullite coated (×) SiC fibers oxidized in flowing oxygen at 1300 °C.

fibers oxidized at 1300 °C in flowing oxygen.[10] The plot shows that the uncoated fibers gained weight due to the formation of SiO_2 at the surface, part of which spalled when the sample was cooled. In contrast, the mullite coated SiC fibers showed almost no weight gain, and exhibited no signs of cracking or spallation after oxidation.

3. Functionally graded coatings

3.1. Need for functionally graded coatings

For very long-term applications, there is concern that the silica content within the mullite coating itself might be susceptible to hot-corrosion and recession during extended exposure to corrosive atmospheres containing NaCl and water vapor. Lee has demonstrated that the silica in plasma sprayed stoichiometric mullite coatings can be preferentially removed when exposed to recession conditions, leaving behind an alumina skeleton.[6] There is thus strong motivation to substantially reduce or even virtually eliminate the silica component from the surfaces of mullite coatings that are in direct contact with atmospheres containing corrosive oxides and steam. This requires a gradation in the composition of CVD mullite coatings, with the alumina content increasing towards the coating surface. The advantages of this approach include a CTE match at the interface between mullite and the Si-based ceramics and improved corrosion and recession resistance of the alumina-rich coating surface in contact with the corrosive atmospheres, while eliminating abrupt changes in coating composition and phase, resulting in a reduction of growth stresses during deposition and thermal stresses on temperature cycling. Thus, these compositionally graded coatings on Si-based ceramics are expected to have the hot-corrosion and recession resistance of alumina coatings, while maintaining the thermal shock resistance of mullite coatings.

3.2. Kinetics of mullite deposition

In order to functionally grade the composition of the coating, the gas-phase composition will have to be varied during deposition. Thus, the effects of deposition parameters on the growth rate and microstructure of the coatings were examined.

A significant increase in the growth rate of the coatings with deposition temperature was observed, consistent with an Arrhenius temperature dependence of growth rate. The increase in the growth rate with temperature also leads to an increase in the coating grain size with temperature (Fig. 4b and c). Interestingly, a decrease in the coating deposition rate was observed when the

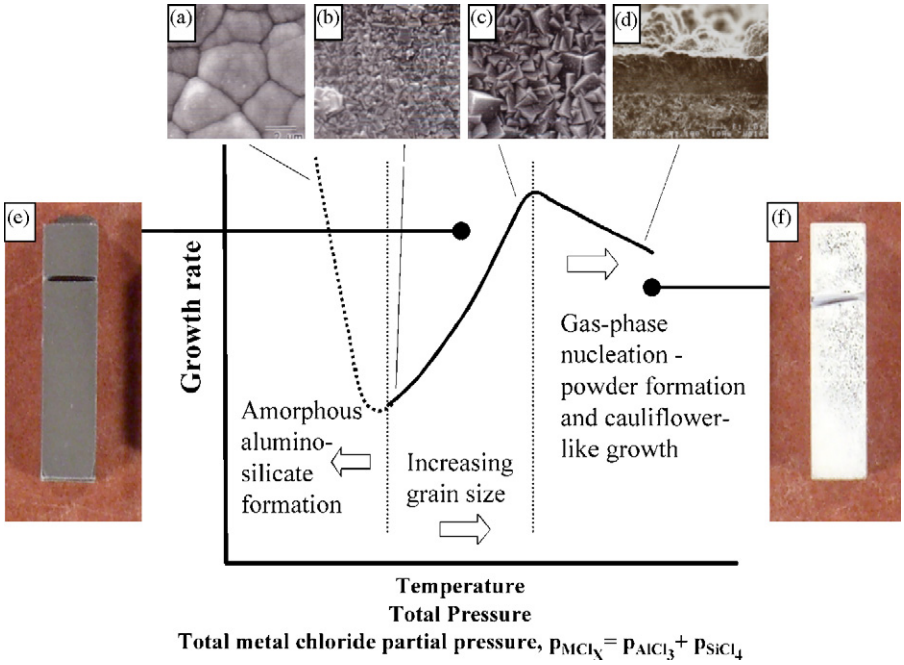

Fig. 4. Schematic of the variation of growth rate of CVD mullite coatings with increasing deposition temperature, total reactor pressure and total metal chloride partial pressure. (a) At low total metal chloride partial pressures, very fast growing amorphous aluminosilicates can form. Increasing the total metal chloride partial pressure leads to (b) crystalline mullite, whose (c) grain size increases with temperature, pressure and total metal chloride partial pressure. (d) However, further increase in these parameters lead to a decrease in deposition rate due to gas-phase nucleation and cauliflower-like outgrowths in the coatings. (e) Sample with no gas-phase powder formation. (f) Sample with excessive gas-phase powder formation.

deposition temperature was increased above 980 °C. This was due to a substantial increase in gas-phase powder formation. The gas-phase powder formation leads to a rapid depletion of the input constituents in the gas phase, leading to a decrease in the coating deposition rate. Although, in general, heterogeneous nucleation on the substrate is preferred, with increasing temperatures, the rate of homogeneous gas-phase nucleation can become significant.[11]

A significant increase in the deposition rate of the coatings with increasing total reactor pressure was found up to a total pressure of 75 Torr. Further increase in the total pressure led to a decrease in the coating deposition rate. It is likely that at the low deposition pressures, the growth is controlled by transport of gaseous species through the boundary layer. Increasing the overall pressure increases the flux through the boundary layer resulting in an increase in the deposition rate. Also, the CVD deposition system increases the total reactor pressure at a constant volumetric flow rate by decreasing the speed of gas removal. Since the residence time of the gaseous species in the reaction zone of the hot-wall CVD reactor is inversely proportional rate of removal, an increase in the total pressure corresponds to an increase in the residence time of the gases.[11] This increase in the residence time would also lead to enhanced growth rates. The increase in growth rates is also reflected in a clear increase in the coating grain size with increasing total reactor pressure. However, further increase in the total pressure to 100 Torr led to a decrease in the coating deposition rate due to gas-phase nucleation of powders accompanied by cauliflower-like growth features on the coating surface (Fig. 4d).

The effect of the total metal chloride partial pressure ($AlCl_3 + SiCl_4$) was studied at a fixed ratio of $AlCl_3/SiCl_4$ of 3:1, which allows the gas-phase Al/Si concentration to be that of stoichiometric mullite. It was found that at very low total metal chloride partial pressures, the growth rate is very high (Fig. 4a). X-ray diffraction studies revealed that the coatings were non-crystalline aluminosilicates. Increasing the total metal chloride partial pressure above a critical value led to a drastic reduction of the growth rate due to the formation of crystalline mullite. Typically, crystalline phases have a slower growth rate since adsorbed atoms needs to be placed in an ordered sequence, as compared to non-crystalline phases. Further increase in the total metal chloride partial pressure led to a modest increase in the growth rate due to the increased availability of the reactant species in the gas phase. When the total metal chloride partial pressure was increased even further, a decrease in the coating deposition rate was observed, accompanied by the onset of excessive gas-phase nucleation.

The effect of deposition temperature, pressure and total metal chloride partial pressure is summarized in Fig. 4. Fig. 4e and f shows a desired coated sample with no powder formation, and a coated sample with significant gas-phase powder formation, respectively.

The effect of the input gas-phase metal chloride ratio (ratio of partial pressures of $AlCl_3$ to $SiCl_4$ at a fixed total metal chloride partial pressure of 0.315 Torr) was also studied and the results are shown in Fig. 5. The figure shows that increasing the gas-phase $AlCl_3/SiCl_4$ ratio to 4, increases the deposition rate. A further increase in the $AlCl_3/SiCl_4$ ratio leads to a decrease in the deposition rate due to gas-phase nucleation, accompanied by cauliflower-like outgrowths at the coating surface.

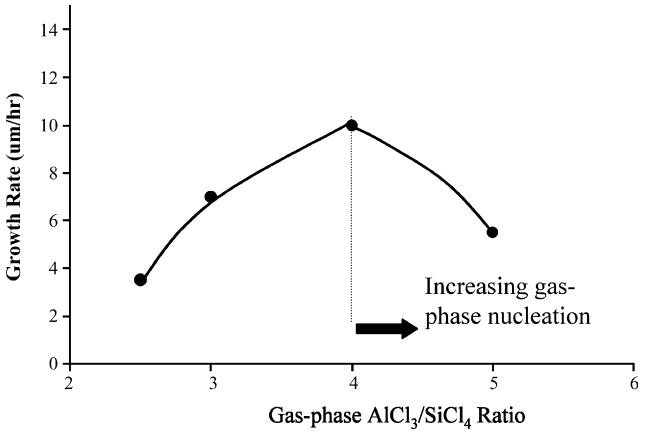

Fig. 5. Plot of coating growth rate as a function of the gas-phase $AlCl_3/SiCl_4$ ratio, at a constant total metal chloride partial pressure of 0.315 Torr ($T = 975$ °C, total pressure = 75 Torr). The growth rate increases as the gas-phase $AlCl_3/SiCl_4$ ratio is increased to 4, after which the coating growth rate decreases with accompanying gas-phase powder formation.

3.3. Microstructure of graded mullite coatings

It was found that mullite coatings can be grown with a range of input $AlCl_3/SiCl_4$ ratios.[12] This is consistent with numerous reports in the literature that the solid solution range in the alumina–silica phase diagram can be extended significantly into the alumina-rich regime.[13–15] The change in the gas-phase composition in the CVD reactor leads to a change in the surface composition of the growing coating. By varying the $AlCl_3/SiCl_4$ input ratio during growth, the coating composition can be graded, as shown in Fig. 6a (the composition is expressed as the Al/Si ratio, with the stoichiometric Al/Si ratio in mullite being 3). It was found that when the composition was graded, mullite grains do not nucleate during deposition unless the surface composition of the growing coating is within a narrow range of 3.2 ± 0.3,[16,17] which is close to the value of stoichiometric mullite. When the surface composition is below this range, co-deposition of nano-sized (~5 nm) γ-Al_2O_3 crystallites (SAED pattern shown in Fig. 6c) in a vitreous silica matrix occurs. Fig. 6b shows the TEM micrograph of such a 'nanocrystalline' layer. Fig. 7 shows a TEM cross-sectional micrograph of the nanocrystalline/crystalline interface, showing that there is a small change in the Al/Si ratio at the interface, and that the transition composition is in the narrow range close to stoichiometric mullite. Once nucleated, columnar mullite grains (Fig. 6d) can grow over a wide range of increasing alumina-rich compositions. The accompanying selected area electron diffraction (SAED) pattern from a coating grain in Fig. 6e is consistent with the [0 1 0] zone axis of mullite.[18] Fig. 6d shows that the vector ***2s***, between the superlattice spots centered around the $\{h\,0\,l\}$ reciprocal lattice projection is aligned along the a^* direction. This has been attributed to the formation of an incommensurate antiphase domain structure due to

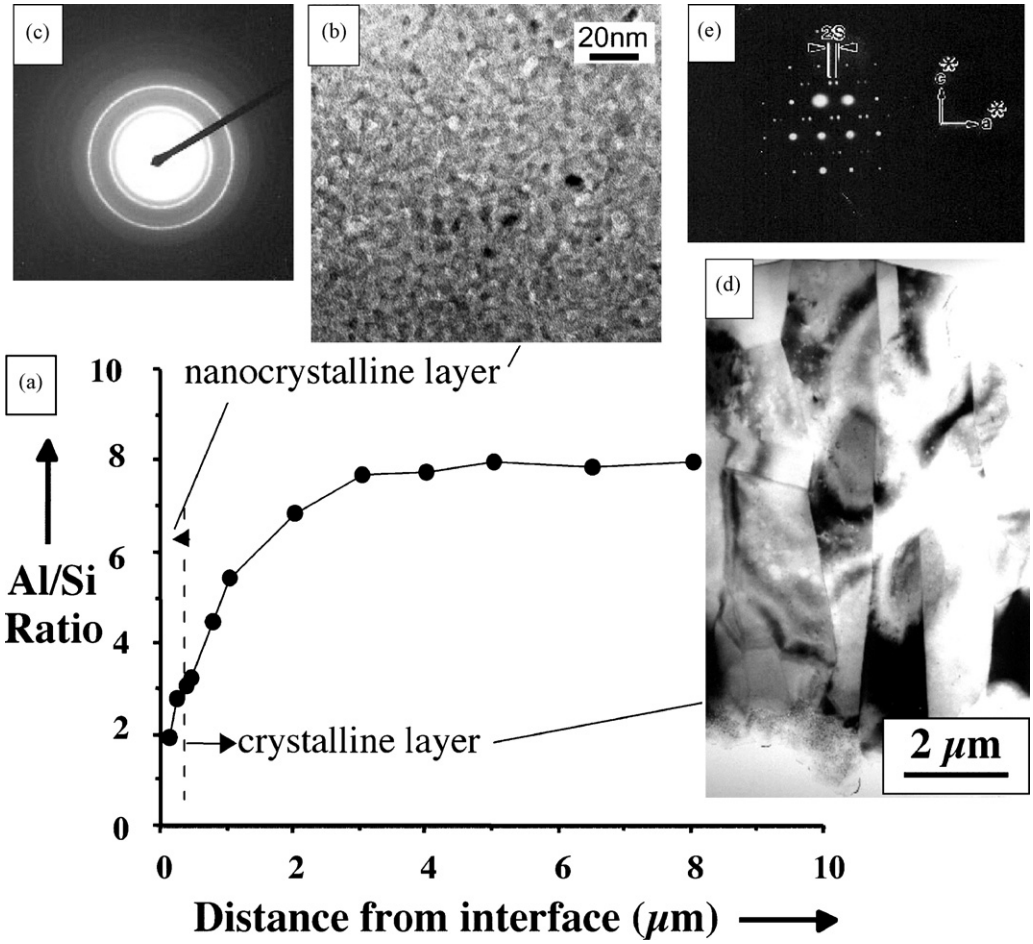

Fig. 6. (a) Composition (expressed as the Al/Si ratio) gradation across a functionally graded CVD mullite coating. The surface of this coating has an Al/Si ratio of 8. (b) Cross-sectional TEM micrograph of the nanocrystalline layer showing 5 μm crystallites. (c) SAED pattern of γ-Al_2O_3 in the nanocrystalline layer. (d) Cross-sectional TEM micrograph showing the columnar mullite grains with increasing Al/Si ratio in the crystalline layer of the as-deposited coating. (e) [0 1 0] mullite SAED pattern from a mullite grain, showing superlattice spots with spacing **2s**.

ordering of oxygen vacancies.[19] The orientation of the ***2s*** vector indicates that these antiphase boundaries (APBs) are oriented parallel to (1 0 0), which is commonly reported for mullite compositions that are not very alumina rich. The nanocrystalline region gets converted to mullite on annealing at temperatures of 1100 °C and above without any microcracking, or porosity formation.[4]

3.4. Properties of functionally graded coatings

The functionally graded mullite coatings were subjected to 500 one-hour thermal cycles 1250 °C and room temperature. There was no evidence of blistering, cracking or spallation of the coating after the cyclic oxidation test, indicating excellent coating adhesion.[4] Fig. 8a shows a cross-sectional TEM micrograph of the high alumina coating surface (Al/Si ∼ 8), which exhibited no signs of phase separation after 500 h at 1250 °C. However, after a 100 h anneal at 1400 °C, α-Al_2O_3 precipitates were formed in the very high alumina-rich regions (6 < Al/Si < 8). It is important to note that this precipitation was not accompanied by any cracking (Fig. 8b). In addition, irregular lamellae of twinned mullite (Fig. 9a), 20–100 nm in width, were seen in these high alumina regions. Fig. 9b also shows a [0 1 0] SAED pattern from the twinned region. The SAED pattern shows that the twin planes are aligned along (0 0 1), in agreement with the observations of Kriven and Pask[14] and Nakajima and Ribbe.[19] Fig. 9c, a schematic of the indexed SAED pattern, shows that four superlattice spots appear around the $\{h\,0\,l\}$ positions in the SAED pattern from the twinned region. One pair of the superlattice spots (e1-type) is related to a twin, while the other pair (e2-type) is related to the other twin. In twinned mullite, the ***2s*** vector joining the 'e1-type' diffraction spots also has a c^* component that increases with increasing Al/Si ratio in the mullite. The increased c^* component of the ***2s*** vector with increasing Al/Si ratio in mullite has been reported previously.[21]

The CVD mullite coatings were also tested against corrosion attack by an acidic Fe-based coal slag.[21] The uncoated SiC substrates suffered severe material loss and pitting due to coal slag corrosion after a 300 h exposure at 1260 °C (Fig. 10a). In contrast, ∼10 μm thick, uniform CVD mullite coatings were found to be very effective in protection against pitting by coal slag corrosion attack (Fig. 10b). The coating did not degrade in the presence of the liquid slag and did not allow liquid slag seepage

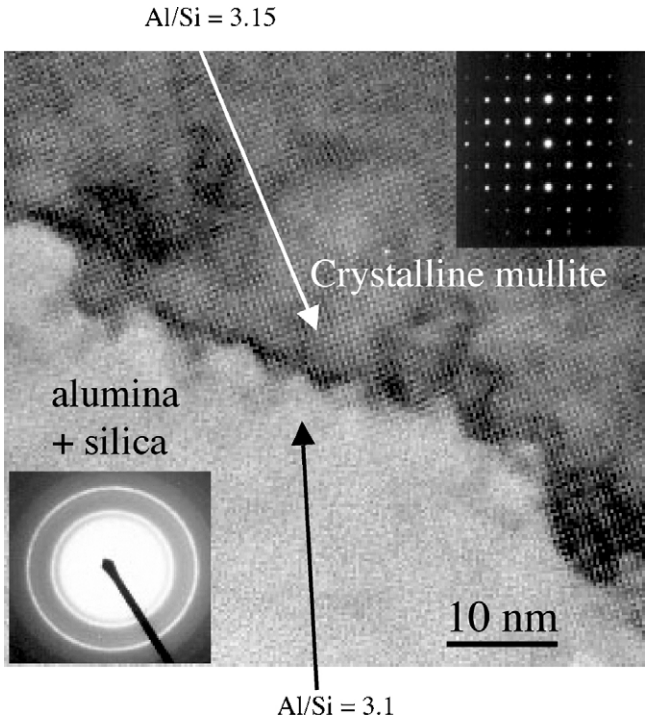

Fig. 7. HRTEM micrograph of the nanolayer/crystalline mullite interface with accompanying SAED patterns from both areas. The composition at which the crystalline mullite nucleates is close to stoichiometric mullite.

to the SiC substrate. These results clearly demonstrate that CVD mullite coatings can provide excellent protection to Si-based ceramics, both under oxidation and hot-corrosion conditions.

3.5. Growth of highly alumina-rich mullite compositions

In the CVD deposition process, once mullite grains nucleate, the mullite structure may be sustained during growth to high Al/Si ratios not attainable by other processes that rely on high activation energy bulk diffusion between alumina and silica during post-deposition annealing. In CVD, the rapid, low-activation energy surface diffusion of the ad-atoms, allow them to use the coating grain as a template for continued growth, even when the ratio of the arrival rates of the Al and Si containing species is far from the stoichiometric value. To study if it was possible to grow virtually silica-free mullite at the coating surface to achieve ι-alumina (alumina in a mullite structure),[22] the gas-phase composition was adjusted to higher and higher $AlCl_3/SiCl_4$ values during growth. Fig. 5 shows that if this ratio is simply increased by keeping the total metal chloride partial pressure constant, the growth rates would be highly diminished and the powder formation would be highly enhanced at the higher input gas ratios ($AlCl_3/SiCl_4$ partial pressures). This problem had to be alleviated by appropriately adjusting the total metal chloride partial pressure.

Fig. 11a shows a cross-section of such a functionally graded coating, etched to remove the silica phase preferentially. As

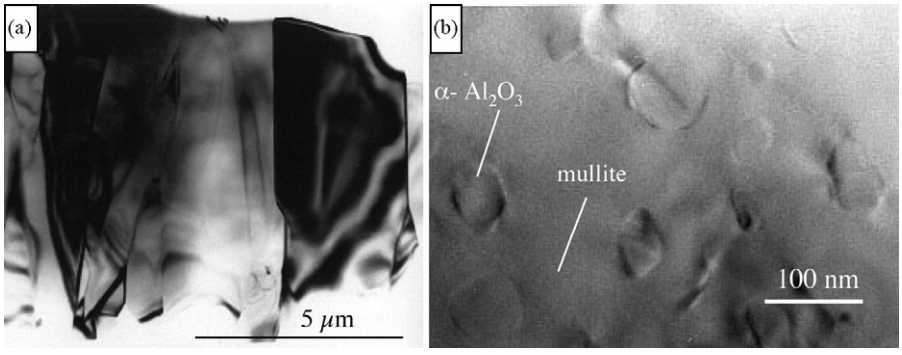

Fig. 8. (a) TEM brightfield micrograph of a high alumina mullite region (Al/Si ~ 8) after 500 h at 1250 °C, showing no phase separation. (b) After 100 h at 1400 °C, α-alumina precipitates form with no cracking.

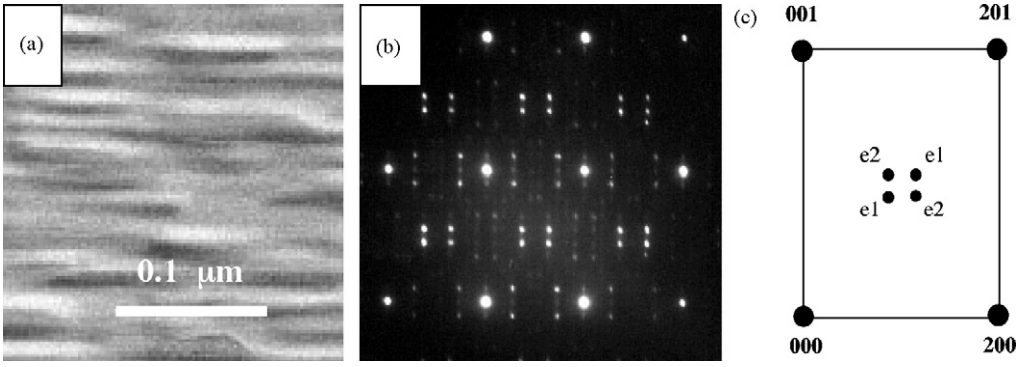

Fig. 9. (a) TEM micrograph showing twin formation in high Al mullite after 100 h at 1400 °C. (b) [0 1 0] SAED pattern of twinned mullite. (c) Schematic of two pairs of superlattice reflections from twinned mullite.

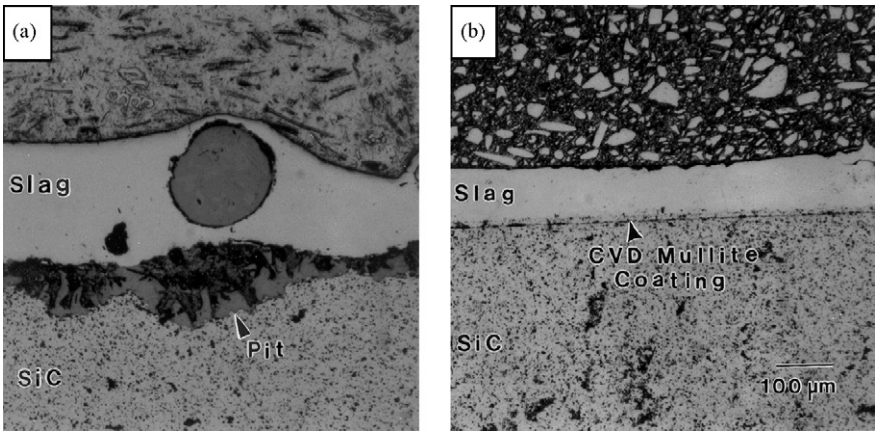

Fig. 10. (a) Optical cross-sectional micrograph of severe pitting in an uncoated SiC substrate exposed to an acidic Fe-based coal slag after 300 h at 1260 °C. (b) A ~10 μm thick CVD mullite coating effectively protected the SiC substrate and eliminated pitting of the substrate.

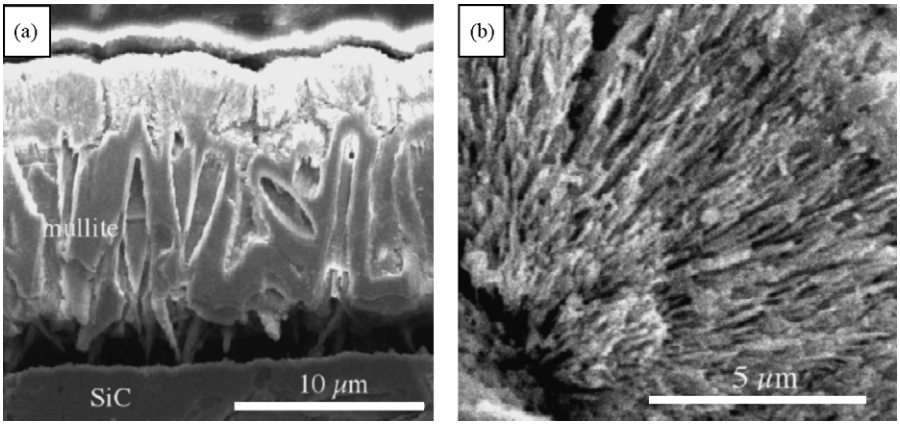

Fig. 11. (a) SEM micrograph of etched cross-section of functionally graded coating. The nanolayer is etched away, and columnar grains can be seen nucleating in the nanolayer. As the Al/Si ratio is increased in the columnar grains, the microstructure changes to a bush-like morphology. (b) Higher magnification of the bush-like structure.

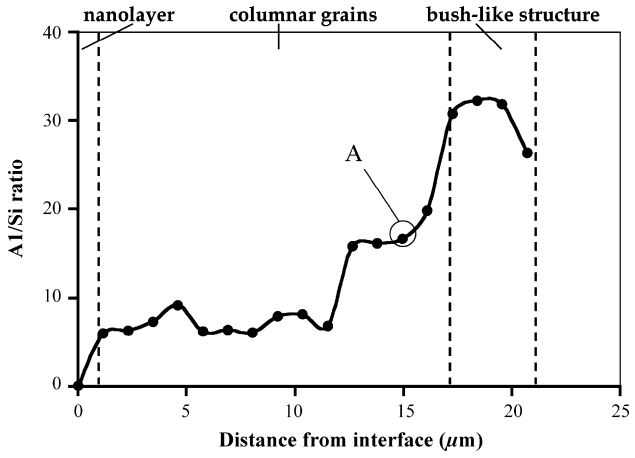

Fig. 12. Composition across the functionally graded coating shown in Fig. 11.

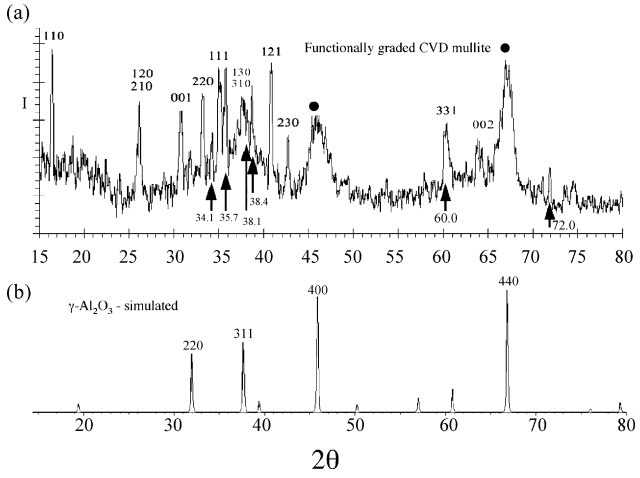

Fig. 13. (a) XRD scan of the functionally graded coating shown in Fig. 11. The indexed peaks belong to mullite, while the peaks marked by arrows belong to the substrate. The peaks marked as by '●' are likely from the bush-like region and appear to be consistent with γ-alumina. (b) Simulated XRD pattern of γ-alumina.

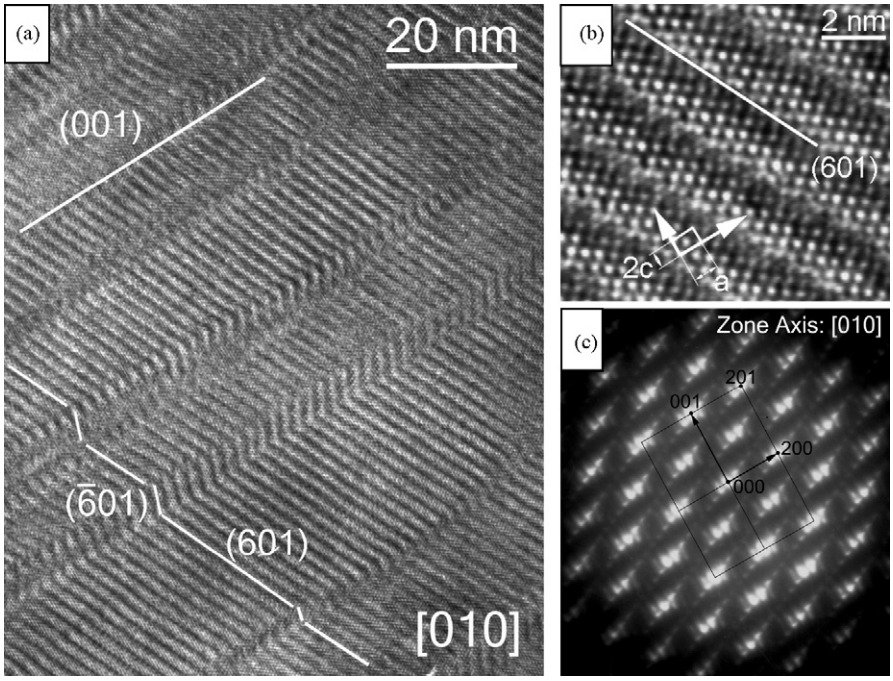

Fig. 14. (a) HRTEM micrograph of a mullite grain oriented along the [0 1 0] zone axis. The composition of this region is marked as A in Fig. 12 (Al/Si ∼ 16), showing a multi-domain region, with two variants of the APB's oriented parallel to (6 0 1) and ($\bar{6}$ 0 1). (b) HRTEM micrograph of the APB's oriented along (6 0 1). (c) [0 1 0] SAED diffraction of the high alumina mullite.

seen in the figure, the nanolayer adjacent to the interface has been etched away, and columnar mullite grains can be seen nucleated in the nanolayer. As seen by the composition profile of the coating in Fig. 12, the Al/Si ratio in the columnar grains increase monotonically until they reach a very high ratio of ∼30. Here, the morphology of the grains changes into bush-like outgrowth of fibrous structures that are submicron in diameter (Fig. 11b).

The θ–2θ XRD scan (Fig. 13) of this coating shows that apart from the substrate and mullite peaks (indexed and marked by arrows, respectively, in Fig. 13a), there are some intense and broad peaks (marked as ● in Fig. 13a) that cannot be indexed as belonging to the mullite structure. The composition in this bush-like region is highly alumina rich with Al/Si ratios in excess of 33. The two broad peaks are consistent with the two strongest peaks of γ-alumina (Fig. 13b), although the other major γ-alumina peaks are obscured by substrate and mullite diffraction peaks. A search of other alumina XRD patterns showed that another little reported metastable alumina phase, δ*-alumina[23] also has two most intense peaks at these locations. Thus, it appears that by changing the input gas metal chloride ratio, the mullite structure can be sustained to very alumina-rich compositions (Al/Si ∼ 30), before the mullite structure breaks down into what is likely an alumina phase with some incorporated Si. The diffraction peaks are consistent with at least two alumina phases (γ and δ*). Detailed TEM analysis of the bush-like structure is currently underway, to identify the structure and study the interface of transition from the columnar to the bush-like structure.

The columnar grains in Fig. 11a were studied by high-resolution transmission electron microscopy (HRTEM) using a JEM-2010LaB_6 electron microscope, operated at 200 kV. Fig. 14a shows a [0 1 0] HRTEM micrograph of a mullite grain where the Al/Si ratio is ∼16 (as marked by A in Fig. 12). This is comparable to some of the most alumina-rich mullite reported in the literature.[15] Fig. 14a shows that the entire observed area of this highly alumina-rich mullite consists of a multi-domain region, with two variants of the APB's oriented parallel to (6 0 1) (shown in Fig. 14b) and ($\bar{6}$ 0 1), respectively. Such multi-domain regions have been reported previously,[20] but in highly localized regions, and not in the entire filed of observation. As seen in Fig. 14a, the domain boundaries are aligned along [0 0 1]. The streaking of all SAED diffraction spots from this region in the c^* direction (Fig. 14c) suggests that the domain boundaries are oriented parallel to the (0 0 1) plane. A more detailed study of this structure is currently underway.

4. Conclusions

Dense, adherent and uniform mullite coatings were deposited on SiC substrates with complex geometries by chemical vapor deposition. Increasing the reactor temperature, reactor total pressure and total metal chloride partial pressure led to increased deposition rates and grain sizes, before gas-phase nucleation occurred leading to cauliflower-like growths on the coating surface accompanied by a decrease in the deposition rates. Decreasing the total metal chloride partial pressure too much led to the formation of non-crystalline aluminosilicates at very high deposition rates. Coatings with functionally graded compositions were also deposited, with the composition being close to stoichiometric mullite at the interface, to some of the highest Al-rich mullite reported at the coating surface. It was found that

at Al/Si ratios of ∼16, multi-domain regions with two variants of the APB's oriented parallel to (6 0 1) and (−6 0 1) formed. At an Al/Si ratio of ∼30, the mullite structure broke down and a bush-like outgrowth of fibrous alumina was seen. These functionally graded coatings exhibited excellent adhesion and corrosion resistance.

Acknowledgements

The author would like to acknowledge the contributions of Dr. Michael Auger, Dr. Ping Hou, Dr. Rao Mulpuri, Dr. Arun Pattanaik and Mr. S. Varadarajan. This research has been partially supported by the National Science Foundation under contract No. DMR 0233952.

References

1. Vision 21 Program Plan, *Clean Energy Plants for the 21st Century*. Federal Energy Technology Center, U.S. Department of Energy, 1999.
2. Jacobson, N. S., Corrosion of silicon-based ceramics in combustion environment. *J. Am. Ceram. Soc.*, 1993, **76**(1), 3–28.
3. Robinson, R. C. and Smialek, J. L., SiC recession caused by SiO_2 scale volatility under combustion conditions: I, experimental results and empirical model. *J. Am. Ceram. Soc.*, 1999, **8**(7), 1817–1825.
4. Hou, P., Basu, S. N. and Sarin, V. K., Structure and high temperature stability of compositionally graded CVD mullite coatings. *Int. J. Refract. Met. Hard Mater.*, 2001, **19**(4–6), 467–477.
5. Lee, K. N., Miller, R. A. and Jacobson, N. S., New generation of plasma-sprayed mullite coatings on silicon carbide. *J. Am. Ceram. Soc.*, 1995, **78**(3), 705–710.
6. Lee, K. N., Current status of environmental barrier coatings for Si-based ceramics. *Surf. Coat. Technol.*, 2000, **133–134**(19), 1–7.
7. Sarin, V. K. and Mulpuri, R. P., Chemical Vapor Deposition of Mullite Coatings. U.S. Patent 576,008 (1998).
8. Mulpuri, R. P. and Sarin, V. K., Synthesis of mullite coatings by chemical vapor deposition. *J. Mater. Res.*, 1996, **11**(6), 1315–1324.
9. Varadarajan, S., Pattanaik, A. K. and Sarin, V. K., Mullite interfacial coatings for SiC fibers. *Surf. Coat. Technol.*, 2001, **139**, 153–160.
10. Pattanaik, A. K. and Sarin, V. K., High temperature oxidation and corrosion of CVD mullite coated SiC. In *Surface Modification Technologies XII*, ed. T. S. Sudarshan, T. A. Khor and M. Jeandin. ASM International, Materials Park, OH, 1998, pp. 91–98.
11. Auger, M. L. and Sarin, V. K., A kinetic investigation of CVD mullite coatings on silicon based substrates. *Int. J. Refract. Met. Hard Mater.*, 2001, **19**, 479–494.
12. Auger, M. L. and Sarin, V. K., The development of CVD mullite coatings for high temperature corrosive applications. *Surf. Coat. Technol.*, 1997, **94–95**, 46–52.
13. Schneider, H. and Komarneni, S., *Mullite*. John Wiley and Sons, New York, 2006.
14. Kriven, W. M. and Pask, J. A., Solid solution range and microstructures of melt mullite. *J. Am. Ceram. Soc.*, 1983, **66**(9), 649–654.
15. Fischer, R. X., Schneider, S. and Schmucker, M., Crystal structure of Al-rich mullite. *Am. Miner.*, 1994, **79**, 983–990.
16. Basu, S. N., Hou, P. and Sarin, V. K., Formation of mullite coatings on silicon based ceramics by chemical vapor deposition. *J. Refract. Met. Hard Mater.*, 1999, **16**(4–6), 343–352.
17. Hou, P., Basu, S. N. and Sarin, V. K., Nucleation mechanisms in chemically vapor-deposited mullite coatings on SiC. *J. Mater. Res.*, 1999, **14**(7), 2952–2958.
18. Doppalapudi, D. and Basu, S. N., Structure of mullite coatings grown by chemical vapor deposition. *Mater. Sci. Eng. A*, 1997, **231**, 48–54.
19. Nakajima, Y. and Ribbe, P. H., Twinning and superstructure of Al-rich mullite. *Am. Miner.*, 1981, **66**, 142–147.
20. Yla-Jaaski, Y. and Nissen, H.-U., Investigation of superstructures in mullite by high resolution electron microscopy and electron diffraction. *Phys. Chem. Miner.*, 1983, **10**, 47–54.
21. Auger, M. L., Sengupta, A. and Sarin, V. K., Coal slag protection of SiC with chemically vapor deposited mullite coatings. *J. Am. Ceram. Soc.*, 2000, **83**(10), 2429–2435.
22. Cameron, W. E., Mullite: a substituted alumina. *Am. Miner.*, 1977, **62**, 747–755.
23. Fargeot, D., Mercurio, D. and Dauger, A., Structural characterization of alumina metastable phase in plasma sprayed deposits. *Mater. Chem. Phys.*, 1990, **24**, 299–314.